Thermal Ignition Analysis of a Monodisperse Spray with Radiation

S. S. SAZHIN,* G. FENG, and M. R. HEIKAL
School of Engineering, Faculty of Science and Engineering, The University of Brighton, Brighton BN2 4GJ, UK

I. GOLDFARB, V. GOL'DSHTEIN, and G. KUZMENKO
Department of Mathematics and Computer Sciences, Ben-Gurion University of the Negev, P.O.B. 653, Beer–Sheva 84105, Israel

The system of equations describing the effects of heating, evaporation, and combustion of fuel droplets in a monodisperse spray is simplified assuming that the Nusselt and Sherwood numbers are equal to 2. The radiative energy exchange between fuel droplets surface and gas is described by using the P-1 model with Marshak boundary conditions. The chemical term is presented in the Arrhenius form with the pre-exponential factor calculated from the enthalpy equation, using the Shell autoignition model. The resultant, singularly perturbed system of ordinary differential equations is analyzed, based on the geometrical version of the integral manifold method. The ignition process is subdivided into two stages: droplet evaporation and ignition of the gaseous mixture. Results predicted by the analytical solutions are compared with those predicted by the CFD package VECTIS. It is suggested that the analytical solution underpredicts the evaporation time. A considerably better agreement between the evaporation times predicted by VECTIS and the proposed theory is achieved when the gas temperature is assumed to be equal to the local temperature in the vicinity of droplets. The effects of thermal radiation are significant, especially at high temperatures and with large droplets, and cannot be ignored.

NOMENCLATURE

a	radiation absorption coefficient
$a_{0,1}$	coefficients defined in Eq. (34)
a_s	scattering coefficient
$a_{\theta,r}$	coefficients defined in Eqs. (28) and (29)
A	constant pre-exponential rate factor
A_{f4}	rate of production of the intemediate agent
c'	molar concentration
C_{pg}	specific heat capacity of gas
D_i	binary diffusion coefficient
E	activation energy
f, F, g	coefficients defined in Eqs. (30) and (31)
h	convection heat transfer coefficient
H_L	$\varepsilon_1 r\theta\sqrt{1 + \beta\theta} + \varepsilon_1\varepsilon_3 r^2[(1 + \beta\theta)^4 - 1]$
H_R	$\eta \exp(\theta/1 + \beta\theta)$
h_m	mass transfer coefficient
L	enthalpy of evaporation
n	droplet number density
Nu	Nusselt number
p	pressure or $\ln(1 + \beta\theta)$
Pr	Prandtl number
q	r^3
q_r	heat flux
Q	specific (unit mass) heat of reaction
r	R_d/R_{d0}
R_d	radius of droplets
R_u	universal gas constant
Re	Reynolds number
s	$(\psi r^3/\epsilon_2) + \eta$
Sc	Schmidt number
Sh	Sherwood number
t	time
t_r	$A^{-1} \exp(1/\beta)$
T	temperature

Greek symbols

α	volume fraction
β	$R_u T_{s0}/E$
γ	$\rho_{g0} C_{pg} T_{go}\beta/\rho_{ff} Q_f$
ϵ_d	emissivity of droplets
ϵ_1	$2\epsilon_d/(2 - \epsilon_d)$
ε_1	$4\pi R_{d0} n \lambda_{g0} T_{s0}^{3/2}\beta(\rho_{ff}\alpha_g Q_f A\sqrt{T_{g0}})^{-1} \exp(1/\beta)$
ε_2	$Q_f \rho_{ff}\alpha_g(\rho_l L\alpha_l)^{-1}$
ε_3	$T_{s0}^{5/2} T_{g0}^{1/2} R_{d0}\sigma_1/(\lambda_{g0}\beta)$
η	c_f'/c_{ff}'

*Corresponding author. E-mail: s.sazhin@bton.ac.uk.

0010-2180/01/$–see front matter
PII S0010-2180(00)00237-6

COMBUSTION AND FLAME 125:684–701 (2001)

Published by Elsevier Science Inc.

ψ	Q_f/L
θ	$(T_g - T_{s0})T_{s0}^{-2}ER_u^{-1}$
κ	coefficient defined in Eq. (37)
λ	thermal conductivity
μ	molar mass of fuel
ρ	density
σ	Stefan–Boltzmann constant
σ_1	$\sigma\epsilon_1$
τ	t/t_r
Ω	slow surface

Subscripts

atm	atmospheric
cf	saturated vapor
d	droplet
evap	evaporation
g	gas
f	fuel
ff	overall fuel
l	liquid
r	radiation
s	surface of droplets
w	wall
0	initial values
1	perturbation

INTRODUCTION

The problem of thermal explosion and ignition in a gas containing fuel droplets is a long-standing one and has numerous applications to furnaces, gas turbines and internal combustion engines [1–3]. Over recent years the theoretical analysis of this problem has been mainly based on computational fluid dynamics (CFD) packages [3–5]. This approach has a number of attractive features since it potentially can account for the various heat transfer and combustion processes in a self-consistent way. It does not, however, allow the separation of the contribution of different processes and, as a result, it cannot be particularly helpful in aiding understanding of the relative contributions of these processes. An alternative approach to this problem is based on analytical analyses of the underlying equations in some limiting cases. This approach cannot replace the CFD approach but can effectively complement it. One of these analyses is based on the geometrical asymptotic method of integral manifolds suggested and developed by Babushok and Gol'dshtein [6] and Gol'dshtein and Sobolev [7]. This method has been successfully applied to thermal explosions in a number of papers [8–10]. Goldfarb et al. [8, 9] assumed heat to be transferred to droplets by thermal conduction rather than convection. McIntosh et al. [10] considered the convection heat transfer, but assumed the convective heat and mass transfer coefficients to be constants which were independent of temperature or droplet radii [11]. None of these papers considered the effect of thermal radiation on heat transfer between droplets and gas, a process that is not negligibly small in many practical applications, including diesel engines [12–16].

The present paper discusses a new analytical solution of the underlying equations. Our approach is based on the further development of some ideas originally suggested in [8–10]. In particular, the dependence of the convective heat transfer coefficient on both gas temperature and droplet radii is taken into account. The contribution of the thermal radiation is included based on the P-1 approximation for the thermal radiation transfer with Marshak boundary conditions [17–19]. As in [8–10], all droplets are assumed to have the same radii (monodisperse spray). Most of the analysis of this paper is equally applicable to the thermal explosion of preheated droplets [8, 20] and the thermal ignition of cold droplets in a hot gas [9]. The results of the analysis are mainly applied to the latter problem, which is particularly important in diesel engines, although the model is applicable to the initial stage of ignition process only, before the rapid increase of gas temperature.

BASIC EQUATIONS AND APPROXIMATIONS

The radiative heat exchange between fuel droplets and the surroundings in many industrial environments, including diesel engines, is complicated by the formation of soot. The presence of soot substantially increases the absorptivity and emissivity of gas. As a result, the gas emissivity may exceed the emissivity of walls. Large concentrations of soot allow the gas to be considered as optically thick and hence the differential P-1 model can be applied to model-

ling the thermal radiative transfer [17–19]. This model can be applied even if the condition of large optical thickness is not satisfied (in the initial stage before ignition) although in this case one can expect overprediction of radiative fluxes from localized sources [19]. Assuming that the droplets are opaque, their surfaces are gray, and the so called radiative temperature T_r is equal to gas temperature T_g, the energy balance equation for the gas can be written as [20]:

$$\rho_g C_{pg} \alpha_g \frac{dT_g}{dt} = \eta c'_{ff} \mu_f \alpha_g Q_f A \exp\left(-\frac{E}{R_u T_g}\right) - 4\pi R_d^2 n h (T_g - T_s) - 4\pi R_d^2 n \sigma \epsilon_1 (T_g^4 - T_s^4) \quad (1)$$

where ρ_g is the gas density, C_{pg} the specific heat capacity of gas, α_g the non-dimensional volumetric gas content, $\eta = c'_f/c'_{ff}$ the non-dimensional mole fraction of the combustible gas, c'_{ff} the overall fuel molar concentration, c'_f the fuel molar concentration far from droplets, μ_f the molar mass of fuel ($\rho_f = \mu_f c_f$), Q_f specific (per unit mass) heat of reaction, A a constant pre-exponential rate factor (in s^{-1}), E the activation energy, R_u the universal gas constant, R_d the droplet radius, h the convection heat transfer coefficient, n the droplet number density, $\epsilon_1 = 2\epsilon_d/(2 - \epsilon_d)$, ϵ_d the emissivity of the droplet surfaces, σ the Stefan–Boltzmann constant, T_s the temperature of droplet surfaces. The parameter A has a slightly different meaning when compared with the parameters A used in [8–10].

When deriving Eq. 1 the Marshak boundary condition was assumed at the droplet surfaces [21]. The radiative exchange with semi-transparent droplets was considered in [22–24], but this is beyond the scope of this paper. In the limiting case of an optically thin gas (the start of the combustion process in diesel engines) the same Eq. 1 could be used but with ϵ_1 replaced by ϵ_d and T_r replaced by the wall temperature T_w. The choice of the normalizing factor c'_{ff} ensures that $\eta \leq 1$ [9]. Apart from the last (radiation) term on the right hand side, Eq. 1 is similar to Eq. 1 in McIntosh et al. [10]. When deriving 1 the chemical term is effectively presented in the form appropriate to a one step reaction with A = const [1, 25]. This is justified if the concentration of fuel is assumed to be so small that the percentage of oxygen consumed can be ignored. An alternative simplified presentation of the chemical term has been discussed by Bergeron and Hallett [26]. The value of A is adjusted to give agreement between the reaction rate predicted by the one step reaction and by a more realistic autoignition model (see Appendix). The equation for the radius of a droplet is taken in the form identical to that given by McIntosh et al. [10] [see their Eq. (2)]:

$$\frac{dR_d}{dt} = -\frac{h_m \mu_f (c'_{fs} - c'_f)}{\rho_l}, \quad (2)$$

where ρ_l is the density of the liquid fuel, c'_{fs} the saturated vapor molar concentration, and h_m the mass transfer coefficient.

The equation for the concentration of combustible gas is:

$$\mu_f c'_{ff} \alpha_g \frac{d\eta}{dt} = -\mu_f c'_{ff} \eta \alpha_g A \exp\left(-\frac{E}{R_u T_g}\right) + 4\pi R_d^2 n h_m \mu_f (c'_{fs} - c'_f). \quad (3)$$

In Eqs. 1–3 it is implicitly assumed that the Spalding number is small, a reasonable assumption when the molar fraction of fuel is small. The latter assumption was already used when we presented the chemical term in the one step reaction form with A = const.

The characteristic times of droplet, t_d, and gas, t_g, heating can be estimated as

$$t_d = C_l \rho_l R_{d0}^2/(3\lambda_{g0})$$

$$t_g = C_{pg} \rho_{g0} T_{g0}/(c'_f \mu_f Q_f A) \exp(E/(R_u T_{g0})).$$

The first expression assumes the droplets to be heated mainly by convection and their temperature is similar to that of the gas. The second expression assumes that the leading contribution comes from the chemical term. For the typical diesel engine parameters $t_d \ll t_g$ and the droplet heating can be neglected [10]. This outcome allows the approximation T_s = const, justified by rigorous numerical simulation of heating and evaporation of fuel droplets, as discussed later, and supported by experiments [27, 28].

When analyzing Eqs. 1–3 without radiation terms McIntosh et al. [10] assumed that ρ_g, h,

and h_m are constants which depend on neither the droplet radii nor the temperature of the surrounding gas. These assumptions are not used in our analysis. Restricting the analysis to the case of constant pressure, $\rho_g = \rho_{g0} T_{g0}/T_g$, where ρ_{g0} is the gas density at the initial temperature T_{g0}. Introducing Nusselt and Sherwood numbers $h = \lambda_g \mathrm{Nu}/2R_d$, $h_m = D_i \mathrm{Sh}/2R_d$, where λ_g is the gas thermal conductivity and D_i the binary diffusion coefficient. The thermal conductivity of both monoatomic and polyatomic gases is proportional to $\sqrt{T_g}$ [29]. The temperature dependence of the specific heat is ignored, while D_i is proportional to $T_g^{3/2}$ and inversely proportional to p [11]. Hence:

$$\lambda_g = \lambda_{g0} \sqrt{\frac{T_g}{T_{g0}}}, \tag{4}$$

$$D_i = \frac{D_{i0} p_{\mathrm{atm}}}{T_{g0}^{3/2}} \frac{T_g^{3/2}}{p}, \tag{5}$$

where suffix $_0$ indicates values at T_{g0}, and p_{atm} is the atmospheric pressure.

In view of Eqs. 4 and 5 and with Nu = Sh = 2, expressions for h and h_m become:

$$h = \frac{\lambda_{g0}}{\sqrt{T_{g0}}} \frac{\sqrt{T_g}}{R_d}, \tag{6}$$

$$h_m = \frac{D_{i0p}}{R_d} \left(\frac{T_g}{T_{g0}} \right)^{3/2}, \tag{7}$$

where $D_{i0p} = D_{i0p_{\mathrm{atm}}}/p$.

The assumption that Nu = Sh = 2 implies that the droplets are suspended in stationary environment. The relative motion between droplets and gas can be taken into account if we replace λ_{g0} by $2\lambda_{g0}/\mathrm{Nu}$ and D_{i0} by $2D_{i0}/\mathrm{Sh}$, where $\mathrm{Nu} = 2.0 + 0.6\mathrm{Re}^{1/2}\mathrm{Pr}^{1/3}$ and $\mathrm{Sh} = 2.0 + 0.6\mathrm{Re}^{1/2}\mathrm{Sc}^{1/3}$. In the case of diesel engines most droplets are entrained in the flow of air/fuel vapor mixture, except in the immidiate vicinity of the nozzles, where the relative velocities of the small droplets are small, $\mathrm{Re} \ll 1$. With $\mathrm{Pr} \approx 0.7$ for air and $\mathrm{Sc} \approx 2$ for the diffusion of heptane in air [30] (data for diesel fuel vapor is not available), $0.6\mathrm{Re}^{1/2}\mathrm{Pr}^{1/3} \ll 1$ and $0.6\mathrm{Re}^{1/2}\mathrm{Sc}^{1/3} \ll 1$. This justifies the application of the model to diesel engines.

From Eqs. 6 and 7, Eqs. 1–3 can be written in dimensionless forms as:

$$\gamma(1 + \beta\theta)^{-1} \frac{\mathrm{d}\theta}{\mathrm{d}\tau} = \eta \exp \frac{\theta}{1 + \beta\theta} - \varepsilon_1 r \theta (1 + \beta\theta)^{1/2} - \varepsilon_1 \varepsilon_3 r^2 [(1 + \beta\theta)^4 - 1], \tag{8}$$

$$\frac{\mathrm{d}r^3}{\mathrm{d}\tau} = -\varepsilon_1 \varepsilon_2 \theta r (1 + \beta\theta)^{1/2} - \varepsilon_1 \varepsilon_2 \varepsilon_3 r^2 [(1 + \beta\theta)^4 - 1], \tag{9}$$

$$\frac{\mathrm{d}\eta}{\mathrm{d}\tau} = -\eta \exp \frac{\theta}{1 + \beta\theta} + \varepsilon_1 \psi r \theta (1 + \beta\theta)^{1/2} + \varepsilon_1 \varepsilon_3 \psi r^2 [(1 + \beta\theta)^4 - 1], \tag{10}$$

where $\gamma = \rho_{g0} C_{pg} T_{go} \beta / \rho_{ff} Q_f$, $\beta = R_u T_{s0}/E$, $\theta = (T_g - T_{s0}) T_{s0}^{-2} E R_u^{-1}$, $\tau = t/t_r$, $t_r = A^{-1} \exp(1/\beta)$, $\varepsilon_1 = 4\pi R_{d0} n \lambda_{g0} T_{s0}^{3/2} \beta (\rho_{ff} \alpha_g Q_f A \sqrt{T_{g0}})^{-1} \exp(1/\beta)$, $r = R_d/R_{d0}$, $\varepsilon_2 = Q_f \rho_{ff} \alpha_g (\rho_l L \alpha_l)^{-1}$, $\varepsilon_3 = T_{s0}^{5/2} T_{g0}^{1/2} R_{d0} \sigma_1 / (\lambda_{g0} \beta)$, $\psi = Q_f/L$, $\sigma_1 = \sigma\epsilon_1$, $\rho_{ff} = c'_{ff} \mu_f$, $\alpha_l = (4/3)\pi R_d^3 n$ is the volume concentration of liquid fuel droplets.

Parameters β and γ are conventional parameters in the Semenov theory of thermal explosion and their physical meanings are well-known [31, 32]; β is the reduced initial temperature (with respect to so-called activation temperature E/R_u) and γ represents the final dimensionless adiabatic temperature of the thermally insulated system after explosion. Characteristic values of both these parameters are small compared with unity for most gaseous mixtures, because of the high exothemicity of the chemical reaction and the high activation energy. The parameters ε_1, ε_2 describe the interaction between gaseous and liquid phases. The parameter ε_3 describes the impact of thermal radiation and represents the ratio of radiative and convective heat transfer coefficients [20]. Characteristic values of ψ lie in the range 10–100.

Apart from the difference in the definitions of η, ε_3 and θ, Eqs. 8–10 are identical to those used in [20]. Initial conditions for Eqs. 8–10: $\theta = \theta_0 = \theta(T_{g0})$, $\eta = \eta_0 = c'_{f0}/c'_{ff}$ and $r = 1$ when $\tau = 0$. These are more general than those used in [8] where it was assumed $T_s = T_{g0}$ at $\tau = 0$. The case of $T_{g0} > T_s$, but without thermal radiation, was considered in [9]. The

latter approximation describes droplet ignition and is applicable when cold droplets are injected into hot gas.

The energy integral for the Eqs. 8–10 can be written as:

$$\eta = \eta_0 - \frac{\gamma}{\beta} \ln\left(\frac{1 + \beta\theta}{1 + \beta\theta_0}\right) + \frac{\psi - 1}{\varepsilon_2}(1 - r^3). \tag{11}$$

Combination of Eqs. 8 and 11 gives:

$$\gamma(1 + \beta\theta)^{-1}\frac{d\theta}{d\tau} = \left[\eta_0 - \frac{\gamma}{\beta}\ln\left(\frac{1 + \beta\theta}{1 + \beta\theta_0}\right) + \frac{\psi - 1}{\varepsilon_2}(1 - r^3)\right] \cdot \exp\frac{\theta}{1 + \beta\theta} - \varepsilon_1 r\theta(1 + \beta\theta)^{1/2} - \varepsilon_1\varepsilon_3 r^2[(1 + \beta\theta)^4 - 1]. \tag{12}$$

Eqs. 8–10 allow steady state conditions to be found. It is expected that once droplet evaporation and gaseous combustion have been completed, then $r = \eta = 0$. This allows the final temperature to be found as:

$$\theta_{\text{final}} = \frac{1}{\beta}\left\{\exp\left[\frac{\beta}{\gamma}\left[\eta_0 + \frac{\psi - 1}{\varepsilon_2}\right] + \ln(1 + \beta\theta_0)\right] - 1\right\}. \tag{13}$$

ANALYSIS

Dynamics of the System

In Eq. 8 the chemical reaction term is exothermic, whereas the heat transfer terms are endothermic. In Eq. 10 the chemical reaction term depletes the fuel vapor, whereas the heat transfer terms produce it. The two-phase mixture is a multiscale system with differences in characteristic relaxation times of the different physicochemical processes. Equations 8–10 are a singularly perturbed system of ODEs, a system with small parameters before the derivatives.

The advantage of this system is that it can be analysed by subdividing it into a number of consequent steps. The relative rates of change of the variables are estimated, to ascertain which are fast and which are slow. The system is shown to be bi-hierarchical and essential features are presented by the method of integral manifolds. Finally, the method is applied to the analysis of the dynamics of the system.

Multiscale System

Eqs. 8–10 can be rewritten in the form:

$$\gamma(1 + \beta\theta)^{-1}\frac{d\theta}{d\tau} = H_R(\theta, \eta) - H_L(\theta, \eta, r), \tag{14}$$

$$\frac{d(r^3)}{d\tau} = -\varepsilon_2 H_L(\theta, \eta, r), \tag{15}$$

$$\frac{d\eta}{d\tau} = -H_R(\theta, \eta) + \psi H_L(\theta, \eta, r), \tag{16}$$

where $H_R(\theta, \eta)$ and $H_L(\theta, \eta, r)$ indicate the chemical heat release and the heat loss because of convection and radiation; these parameters are defined as:

$$H_R(\theta, \eta) = \eta \exp\left(\frac{\theta}{1 + \beta\theta}\right);$$

$$H_L(\theta, \eta, r) = \varepsilon_1 r\theta\sqrt{1 + \beta\theta} + \varepsilon_1\varepsilon_3 r^2[(1 + \beta\theta)^4 - 1].$$

With the new variables: $p = \ln(1 + \beta\theta)$; $q = r^3$; $s = (\psi r^3/\varepsilon_2) + \eta$ Eqs. 14–16 simplify to:

$$\frac{\gamma}{\beta}\frac{dp}{d\tau} = H_R(\theta, \eta) - H_L(\theta, \eta, r), \tag{17}$$

$$\frac{1}{\varepsilon_2}\frac{dq}{d\tau} = -H_L(\theta, \eta, r), \tag{18}$$

$$\frac{ds}{d\tau} = -H_R(\theta, \eta), \tag{19}$$

where (θ, η, r) on the right of Eqs. 17–19 are functions of p, q, and s.

For typical values of parameters for a diesel engine, the inequalities $1/\varepsilon_2 \ll \gamma/\beta < 1$ hold (for values of parameters discussed later $\gamma/\beta = 0.268$, $1/\varepsilon_2 = 0.0058$ for $T_{s0} = 600$ K and $1/\varepsilon_2 = 0.0084$ for $T_{s0} = 300$ K). This allows the

differences in the values of $1/\varepsilon_2$, γ/β, and unity to be taken into account and different scales of characteristic times to be introduced in Eqs. 17–19, creating a bi-ierarchy in this system of equations: the variable q is fast, the variable p is intemediate and the variable s is slow.

A number of asymptotic methods can be applied for qualitative study of multi-scale systems of this type. The approach adopted decomposes the multiscale system into so called 'fast' and 'slow' subsystems on the 'fast' and 'slow' integral manifolds. The advantage of this is that these integral manifolds have lower dimensions than the original problem.

Method of Integral Manifolds

A general theory of integral manifolds was developed for non-linear mechanics and has been described in detail in the books [33, 34], as well as the paper [35]. An original geometrical version of the general integral manifolds approach was adopted for the stiff problems of chemical kinetics and combustion by Gol'dshtein and Sobolev [7]. The high efficiency of this mathematical tool has been demonstrated in a variety of applications and results appear in [8–10] and [20].

To demonstrate the essence of this approach a singularly perturbed system of ordinary differential equations is considered:

$$\frac{\mathrm{d}x}{\mathrm{d}t} = F(x, y) \tag{20}$$

$$\epsilon \frac{\mathrm{d}y}{\mathrm{d}t} = G(x, y), \tag{21}$$

where x and y are n- and m-dimensional vector variables, and $\epsilon \ll 1$ is a positive parameter.

According to a standard definition [34] a manifold (surface) $M := \{(x, y) : y = h(x, \epsilon)\}$ is an integral manifold of the Eqs. 20–21 if any phase trajectory $\gamma(x, y)$ of the Eqs. 20–21 intersecting with M belongs to M in the domain of existence of M. The general theory of integral manifolds states that integral (invariant) manifolds M belong to the ϵ-neighborhood of the slow (quasistationary) manifold $M_0 := \{(x, y) : y = h_0(x)\}$, where $y = h_0(x)$ is an isolated solution of Eq. 21 with $\epsilon = 0$:

$$G(x, h_0(x)) = 0. \tag{22}$$

Moreover there exists a unique representation of $h(x)$ as an asymptotic series with respect to the small parameter ϵ:

$$h(x, \epsilon) = h_0(x) + \sum_{i=1}^{\infty} \epsilon^i h_i(x). \tag{23}$$

An effective analytical algorithm for the evaluation of $h_i(x)$ for an arbitrary i exists (by iteration) and it has been proved that under specific conditions [34] the series converges to the function $h(x, \epsilon)$. The conditions for existence and the uniqueness of the manifold $M := \{(x, y) : y = h(x, \epsilon)\}$ in the ϵ-neighborhood of the slow manifold M can be determined, but the discussion of these aspects is beyond the scope of the present paper, see [34].

The general theory, which has become known as the geometrical asymptotic version of integral manifolds method [33–35], leads to a number of important conclusions. In particular, it can be shown that the slow surface (slow manifold) M_0 is a $O(\epsilon)$ approximation of the integral manifolds, except at the points where the basic assumptions are no longer valid (the so-called turning points). This allows us to write the equation for the slow sub-system Eq. 20 on the slow surface in the form:

$$\frac{\mathrm{d}x}{\mathrm{d}t} = F(x, h_0(x))$$

[which has a lower dimension than the original system, Eqs. (20–21)] and to study the system dynamics on it. The asymptotic series, Eq. 23, is not time-dependent and standard methods of time-dependent asymptotic series are not relevant to its analysis. Asymptotic series of integral manifolds of the type shown by Eq. 23 are asymptotic expansions of 'fast' phase variables based on 'slow' phase variables. This may be interpreted in the following way. Each solution of the system of Eqs. 20–21 can be presented as a trajectory in the phase space of the variables x and y. This trajectory can be subdivided into fast and slow parts. On the fast part, the slow variable x is assumed to be constant (quasi-stationary). On the slow parts, the fast variable y changes with approximately the same rate as the slow one (on the corresponding slow inte-

gral manifold fast and slow processes are balanced). The slow parts of the trajectory are located on the integral manifold M (a curve in the two-dimensional case). For the purpose of qualitative analysis its zero approximation, M_0, can be taken. This means that the application of the technique presented above to the solution of Eqs. 20–21 should start with an estimate of the relative rates of change of the variables and a decision as to which of them are fast and which are slow.

Consider an arbitrary hierarchical level of the system with several characteristic rates of changes. For processes of the same order, all the slower ones are assumed to be 'frozen', whereas all the faster ones are expected to reach their quasi-stationary state. Eventually, however, the processes at the hierarchical level under consideration approach their quasi-stationary state. This state of relative balance is, in general, temporary and these processes can become fast once again [33–35]. This phenomenon is not always well understood and it is sometimes believed that the processes always become quasistationary after the first quasi-relaxation [7].

Application of the Method

The bi-hierarchical behavior of Eqs. 17–19 allows separation of the variables according to their rates of change and application of the method of integral manifolds for the analysis of these equations.

When this system is applied to a diesel engine, the condition $\eta(\tau = 0) = 0$ must be imposed. The term H_R is zero at the beginning of the process as the initial concentration of the gaseous fuel is zero. On the other hand, the initial value of H_L is, in general, large. As already mentioned, for a diesel engine, $1/\varepsilon_2 \ll \gamma/\beta < 1$. Because the right sides of Eqs. 17 and 18 are rather close (as $H_R \ll H_L$), it is to be expected that q changes faster than p from the beginning of the process until such time as H_L becomes small enough (in the zeroth approximation with respect to the small parameter $1/\varepsilon_2$). A similar analysis of Eqs. 17 and 19 shows the variable p to be fast relative to s, since $\gamma/\beta < 1$ and $H_R \ll H_L$ at the beginning of the process. Later, the chemical reaction terms balance the heat transfer terms, due to the temperature rise. Eventually this leads to H_R exceeding H_L. At this stage, explosion of the gaseous mixture can be expected. The two different hierarchies of variables can be recognized: s is the slowest, q the fastest, and p is intermediate.

In general, the analysis of a bi-hierarchal system presents a rather complicated mathematical problem. It includes the study of two different slow manifolds: the slow surface Ω (the variable p is fast and changes, whereas the variables q and s are slow and 'frozen') and the slow curve Λ lying on this slow surface Ω (the variables q and p are fast and change with balanced rates, whereas the variable s is slow and 'frozen'). The analysis of possible trajectories is naturally subdivided into three stages. First we focus on the fast part of the trajectory in which the variable q changes, whereas two others (p and s) conserve their values. This stage is completed when the trajectory reaches the slow surface Ω: the rates of change of the variables q and p become balanced. In accordance with the above analysis the slow surface Ω is determined by $H_L = 0$. Once the trajectory reaches the slow surface it starts to move along it. At the second stage, the direction of motion is determined by the vector field at the point of intersection. The exact location of the trajectory lies in the neighborhood of small $1/\varepsilon_2$ on the slow surface; the trajectory adheres to the slow surface Ω. At this stage the variables p and q are considered as fast, whereas the variable s is considered as slow (it conserves its initial value). This continues until the trajectory intersects the slow curve Λ, defined by the condition $H_L \sim H_R$. At the point of intersection the relative rates of change of all three variables become approximately equal and the trajectory is identified with the slow curve Λ (the third and the last stage of the analysis). This continues until the trajectory approaches the turning point or the steady state of the system (explosion). At this stage, the trajectory reaches the slow surface $H_L = 0$.

It follows from this analysis that the equation for the slow surface Ω can be written as:

$$\Omega = \{(\theta, \eta, r) | H_L = 0\} \tag{24}$$

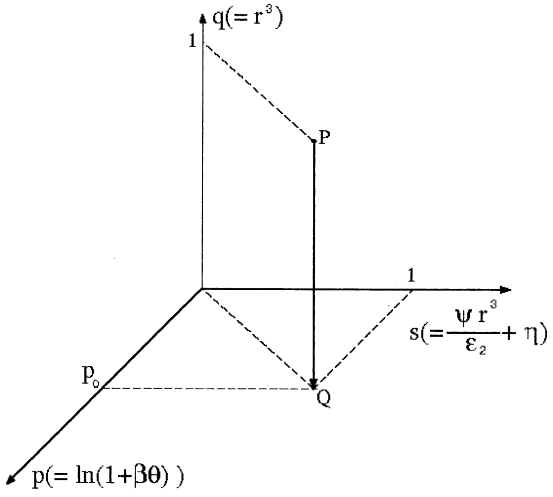

Fig. 1. Schematic view of the (p, q, s) space and the 'fast' trajectory **PQ** in it.

Eq. (24) describes two branches of the slow surface:

$$r = 0 \tag{25}$$

$$\theta\sqrt{1+\beta\theta} + \varepsilon_3 r[(1+\beta\theta)^4 - 1] = 0. \tag{26}$$

The analysis of the vector field in the space (θ, η, r) shows that the first branch is stable and attractive, whereas the second branch has no physical meaning, as it implies that $r < 0$ when $\theta > 0$. In the (p, q, s) space shown in Fig. 1, this first branch reduces to the (p, s) plane. Starting with the initial point **P**, the trajectory moves on this branch parallel (in the zeroth approximation with respect to the small parameter $\beta/\gamma\varepsilon_2$) to the q axis, as shown in Fig. 1. Once the trajectory has reached the slow surface, Eq. 25, at the point **Q** the droplets evaporate ($r = 0$). The s-coordinate of this point is equal to unity as s continues to conserve its initial value. Therefore, $\eta = 1$ as $r = 0$ (evaporation has been completed). The originally formulated problem of thermal ignition in a multiphase medium at this point turns into the conventional problem of a thermal explosion in a flammable gas. The constant value of p indicates that the temperature of the mixture does not change (in the zeroth approximation with respect to the small parameter $\beta/\gamma\varepsilon_2$) at the initial stage of the process (part **PQ** of the trajectory). The problem of finding the curve Λ does not appear in this case.

The slow pace of gas temperature variation during the evaporation process allows us to simplify Eqs. 9 and 12 considerably and obtain their analytical solutions. These are now discussed.

Evaporation Time

It can be assumed that the gas temperature remains close to T_{g0} during the heating, evaporation and initial combustion processes. This approximation allows us to write:

$$\theta = \theta_0 + \theta_1, \tag{27}$$

where $|\theta_1| \ll \theta_0$.

The approximation is justified when the contribution of droplets is sufficiently small. Also, it can be used during the initial stage of combustion, before the actual explosion. This case is particularly important for diesel engines where the evaporation time of droplets and the values of gas temperature, fuel concentration and droplet radii can be estimated before explosion. Analysis of critical conditions for the explosion process requires a different approximation [36].

Having substituted Eq. 27 into Eqs. 12 and 9, and retained only the first order terms the following expressions are obtained:

$$\frac{\mathrm{d}\theta_1}{\mathrm{d}\tau} = a_\theta + b_\theta\theta_1 \tag{28}$$

$$r\frac{\mathrm{d}r}{\mathrm{d}\tau} = a_r + b_r\theta_1, \tag{29}$$

where

$$a_\theta = a_{\theta 0} + a_{\theta 1}r + a_{\theta 2}r^2 + a_{\theta 3}r^3,$$

$$b_\theta = b_{\theta 0} + b_{\theta 1}r + b_{\theta 2}r^2 + b_{\theta 3}r^3,$$

$$a_r = a_{r0} + a_{r1}r, \qquad b_r = b_{r0} + b_{r1}r,$$

$$a_{\theta 0} = \left(\eta_0 + \frac{\psi - 1}{\varepsilon_2}\right)\frac{1+\beta\theta_0}{\gamma}\exp\left(\frac{\theta_0}{1+\beta\theta_0}\right),$$

$$a_{\theta 1} = -\frac{\varepsilon_1\theta_0(1+\beta\theta_0)^{3/2}}{\gamma},$$

$$a_{\theta 2} = -\frac{\varepsilon_1\varepsilon_3(1+\beta\theta_0)[(1+\beta\theta_0)^4 - 1]}{\gamma},$$

$$a_{\theta 3} = -\frac{(\psi - 1)(1 + \beta\theta_0)}{\varepsilon_2 \gamma} \exp\left(\frac{\theta_0}{1 + \beta\theta_0}\right),$$

$$b_{\theta 0} = \left[-1 + \frac{1}{\gamma}\left(1 - \frac{\beta}{1 + \beta\theta_0}\right)\left(\eta_0 + \frac{\psi - 1}{\varepsilon_2}\right)\right] \cdot \exp\left(\frac{\theta_0}{1 + \beta\theta_0}\right),$$

$$b_{\theta 1} = -\frac{\varepsilon_1}{\gamma}\left(1 + \frac{3}{2}\beta\theta_0\right)(1 + \beta\theta_0)^{1/2},$$

$$b_{\theta 2} = -\frac{4\varepsilon_1\varepsilon_3\beta}{\gamma}(1 + \beta\theta_0)^4,$$

$$b_{\theta 3} = -\frac{\psi - 1}{\varepsilon_2\gamma}\left(1 - \frac{\beta}{1 + \beta\theta_0}\right)\exp\left(\frac{\theta_0}{1 + \beta\theta_0}\right),$$

$$a_{r0} = -\frac{\varepsilon_1\varepsilon_2\theta_0(1 + \beta\theta_0)^{1/2}}{3},$$

$$a_{r1} = -\frac{\varepsilon_1\varepsilon_2\varepsilon_3}{3}[(1 + \beta\theta_0)^4 - 1],$$

$$b_{r0} = -\frac{\varepsilon_1\varepsilon_2(1 + \beta\theta_0)^{1/2}}{3}\left[1 + \frac{\beta\theta_0}{2(1 + \beta\theta_0)}\right],$$

$$b_{r1} = -\frac{4\varepsilon_1\varepsilon_2\varepsilon_3\beta}{3}(1 + \beta\theta_0)^3.$$

Rearranging Eqs. 28 and 29 gives:

$$\frac{d\theta_1}{dr} + f\theta_1 = g, \tag{30}$$

where

$$f = \left(\frac{b_r a_\theta}{a_r^2} - \frac{b_\theta}{a_r}\right)r, \qquad g = \frac{r a_\theta}{a_r}$$

The solution of Eq. 30, subject to the boundary condition $\theta_1(r = 1) = 0$ is:

$$\theta_1 = e^{-F}\int_1^r g e^F \, dr, \tag{31}$$

where $F = \int_1^0 f \, dr$. Having substituted Eq. 31 into Eq. 29, the implicit expression for the time dependence of r can be found:

$$\tau = \int_1^r \frac{r \, dr}{a_r + b_r\theta_1(r)}. \tag{32}$$

Assuming that $r = 0$ in Eq. 32, the explicit expression for the time for complete evaporation of the fuel droplet is:

$$\tau_{\text{evap}} = \int_1^0 \frac{r \, dr}{a_r + b_r\theta_1(r)}. \tag{33}$$

This expression is accurate if the condition $|\theta_1| \ll \theta_0$ is satisfied throughout the whole process. If this is not the case, then Eq. 33 gives the upper limit of the physical ignition time delay. The latter is a rough indicator of the total ignition delay time, bearing in mind that the chemical ignition delay time for diesel engines is generally much less than the physical ignition delay time [37].

Once the temporal dependence of temperature and droplet radii are obtained, the time dependence of fuel concentration can be calculated from Eq. 11. With the assumption that $|\theta_1| \ll \theta_0$, the changes in T_g can be ignored when estimating droplet radius. In this case combining Eqs. 2, 6, 7, and the assumption $T_s = \text{const}$ gives:

$$\frac{dr}{dt} = -a_0 - \frac{a_1}{r}, \tag{34}$$

where $r = R_d/R_{d0}$, $a_0 = \sigma\epsilon_1(T_{g0}^4 - T_s^4)/L\rho_l R_{d0}$, $a_1 = \lambda_{g0}(T_{g0} - T_s)/L\rho_l R_{d0}^2$.

Having integrated Eq. 34 then:

$$t = -\int_1^r \frac{r \, dr}{a_0 r + a_1} = \frac{1}{a_0}\left[1 - r + \frac{a_1}{a_0}\ln\frac{a_1 + a_0 r}{a_1 + a_0}\right]. \tag{35}$$

The assumption that the contribution of thermal radiation is small implies that $|a_0| \ll |a_1|$ and Eq. 35 can be simplified to (ignoring the fourth order terms):

$$t = \frac{1}{2a_1}(1 - r^2) - \frac{a_0}{a_1^2}(1 - r^3). \tag{36}$$

The first term in Eq. 36 gives the well known d^2-law for droplet evaporation. The second term describes the correction due to the contribution of thermal radiation.

Assuming $r = 0$ in Eq. 36, an alternative expression for droplet evaporation time can be obtained in the form:

$$t_{\text{evap}} = t_{\text{evap}(0)}(1 - \kappa), \tag{37}$$

where $t_{\text{evap}(0)} = L\rho_l R_d^2/2\lambda_{g0}(T_{g0} - T_s)$ is the evaporation time in the absence of thermal radiation, $\kappa = 2\sigma\epsilon_1 R_{d0}(T_{g0}^4 - T_s^4)/3\lambda_{g0}(T_{g0} - T_s)$ accounts for the effect of this.

APPLICATION TO DIESEL FUEL DROPLETS

Following [37, 38], diesel fuel is approximated by n-dodecane ($C_{12}H_{26}$). It is assumed that the initial droplet radii are equal to $R_{d0} = 6$ μm and all droplets are identical. This enables the analytical results to be employed. It is assumed that once droplets have evaporated, the mixture becomes stoichiometric with an air/fuel mass ratio 11.7. This implies that the number density of droplets is equal to 3.02×10^{12} m^{-3}, which corresponds to $\alpha_l = 2.73 \times 10^{-3}$ if the droplets' temperature is equal to 300 K and their density is equal to 744 kg/m^3 (thermal expansion of droplets was taken into account). The mixture practically never becomes stoichiometric, since the evaporation of droplets is accompanied by their combustion. The initial gas temperature is assumed equal to $T_{g0} = 880$ K and the initial pressure is assumed equal to 6 MPa, to compare the computations with available experimental data. These values of temperature and pressure are higher than those currently used in most diesel engines (cf. Fig. 3.10 of [2]), but reflect current trends [39, 40]. It is assumed that the initial temperature of droplets is equal to 300 K. The heating of the droplets by the surrounding gas increases their temperature until it reaches about 600 K. At this stage, it is expected that the quasistationary approximation becomes valid and it seems reasonable to assume that $T_s = 600$ K. At this temperature, n-dodecane has the physical properties: $C_l = 2.83$ kJ/(kg K), $\rho_l = 600$ kg/m^3, $L = 250$ kJ/kg, $Q_f = 43$ MJ/kg. The molar mass of n-dodecane, μ_f, is equal to 170 kg/kmol. The increase in droplet temperature from 300 to 600 K decreases the density from 744 to 600 kg/m^3. This increases the droplet radius from 6 to 6.445 μm and α_l from 2.73×10^{-3} to 3.39×10^{-3}. For comparison, calculations are also performed for a droplet temperature of 300 K at which n-dodecane has the physical properties: $C_l = 1.655$ kJ/(kg K) and $L = 360$ kJ/kg. The initial density of air at $T_{g0} = 880$ K and $p = 6$ MPa is estimated as: $\rho_{g0} \approx 23.8$ kg/m^3, $C_{pg} = 1.12$ kJ/(kg K), $\lambda_{g0} = 6.1 \times 10^{-2}$ W/(m K). The selected parameters are for a stoichiometric mixture and: $\rho_{ff} = \rho_{g0}/11.7 = 2.034$ kg/m^3, $c'_{ff} = \rho_{ff}/\mu_f = 0.012$ kmol/m^3. Assuming that the emissivity of droplets, ε_d, is equal to 1, $\sigma_1 = 11.3 \times 10^{-8}$ W/(m^2 K^4). Because the volume fraction of droplets is negligible, it is assumed that $\alpha_g = 1$ which implies that $\varepsilon_2 = \psi$. The value of E 76 kJ/mol and three values of A, 10^6 s^{-1}, 5×10^6 s^{-1}, and 10^7 s^{-1} are used, the first value from [26]. The values of A are approximations of the autoignition process by a single step reaction. This modelling is based on the Shell model (see Appendix), the data set gives the values for dimensionless parameters and t_r presented in Tables 1 and 2.

With these values of parameters and $A = 10^7$ 1/s, Eqs. 17–19 were solved numerically for $T_{s0} = 600$ K to obtain the dependence of p, q, and s on τ. The results are shown in Fig. 2. This figure confirms the main results of the analysis,

TABLE 1

Values of β, γ, t_r, $\varepsilon_{1,2,3}$, and ψ for Initial Droplet Surface Temperature 600 K, Initial Gas Temperature 880 K, and A Equal to 10^6, 5×10^6, and 10^7 1/s

A =	10^6 1/s	5×10^6 1/s	10^7 1/s
β =	6.56×10^{-2}	6.56×10^{-2}	6.56×10^{-2}
γ =	1.76×10^{-2}	1.76×10^{-2}	1.76×10^{-2}
t_r =	4.13 s	0.827 s	0.413 s
ε_1 =	22.93	4.586	2.292
$\varepsilon_2 = \psi$ =	172.0	172.0	172.0
ε_3 =	4.758×10^{-2}	4.758×10^{-2}	4.758×10^{-2}

TABLE 2

The Same as Table 1, but for Initial Droplet Surface Temperature 300 K

A =	10^6 1/s	5×10^6 1/s	10^7 1/s
β =	3.28×10^{-2}	3.28×10^{-2}	3.28×10^{-2}
γ =	8.80×10^{-3}	8.80×10^{-3}	8.80×10^{-3}
t_r =	1.71×10^7 s	3.42×10^6 s	1.71×10^6 s
ε_1 =	1.560×10^7	3.119×10^6	1.560×10^6
ε_2 =	119.6	119.6	119.6
ψ =	119.4	119.4	119.4
ε_3 =	1.566×10^{-2}	1.566×10^{-2}	1.566×10^{-2}

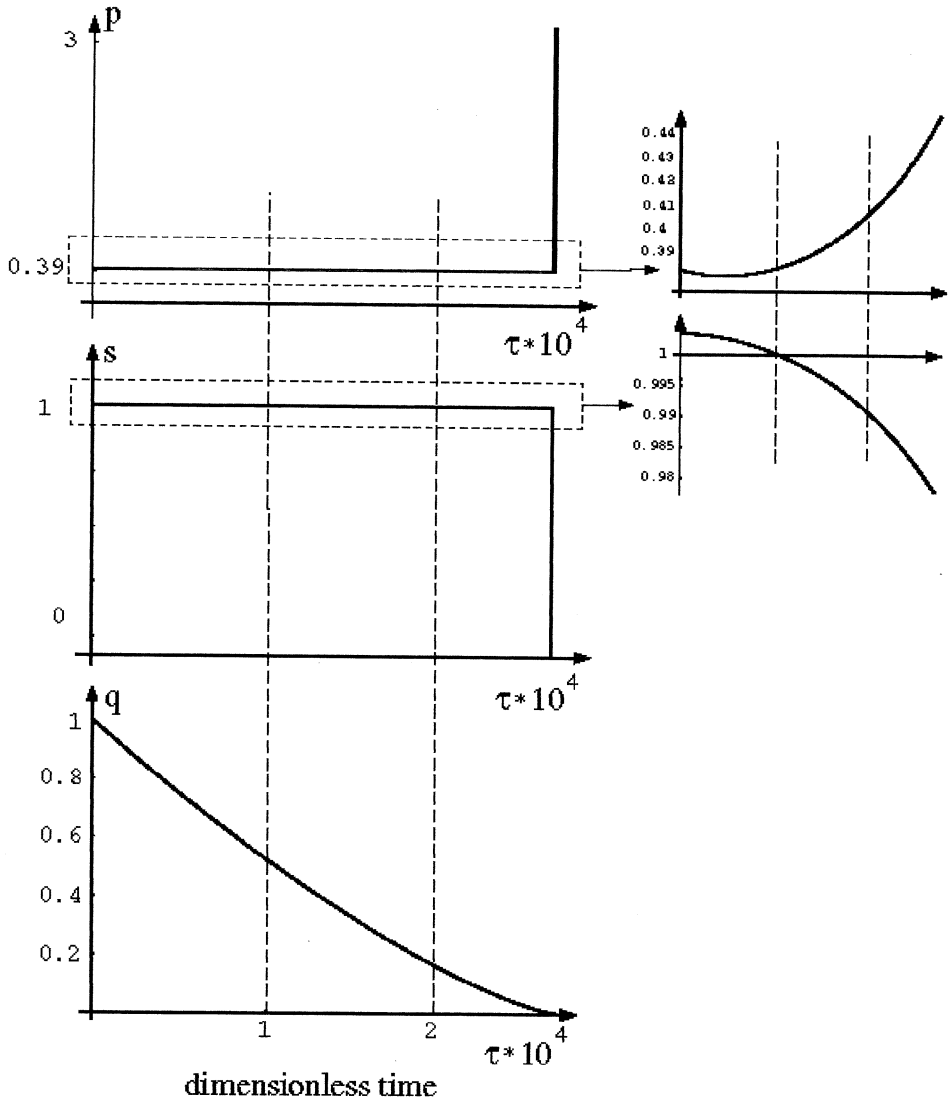

Fig. 2. Plots of p versus τ, q versus τ, and s versus τ as calculated based on numerical solution of Eqs. (17–19) for the values of parameters presented in Table 1, $T_{s0} = 600$ K and $A = 10^7$ 1/s.

presented earlier, regarding the rates of change of p, q, and s. The values of p and s remain almost constant, whereas q decreases from unity to zero. In Fig. 3 the same results are presented, but as plots of θ versus τ, η, versus τ, and r versus τ. The triangles on the same figure show the results of calculations based on the simplified analytical model discussed in the previous section. This figure demonstrates that the predicted results from the analytical model are close to those from the rigorous numerical solution of the underlying equations. This gives additional support to the approximate model.

By using the values of parameters given in Tables 1 and 2, the temporal dependence of gas temperature and droplet diameter have been calculated using Eqs. 31 and 32 and the results are shown in Figs. 4a,b. In Fig. 4b, the plots predicted by Eqs. 35 and 36 (which are not distinguishable within the accuracy of plotting) are also shown. As can be seen from Fig. 4b, the temporal dependence of droplet diameter is a rather weak function of A. All curves are reasonably close to those predicted by Eqs. 35 and 36. The closeness of these curves confirms that thermal radiation effects are small. Based on

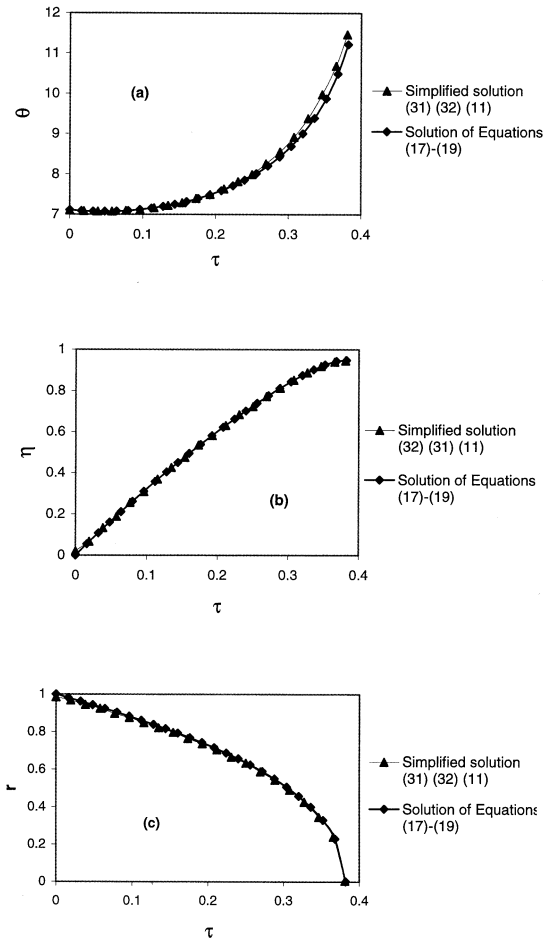

Fig. 3. Same results as in Fig. 2 but as plots of θ versus τ (a), η versus τ (b), and r versus τ (c). Triangles show results based on Eqs. (31), (32), and (11).

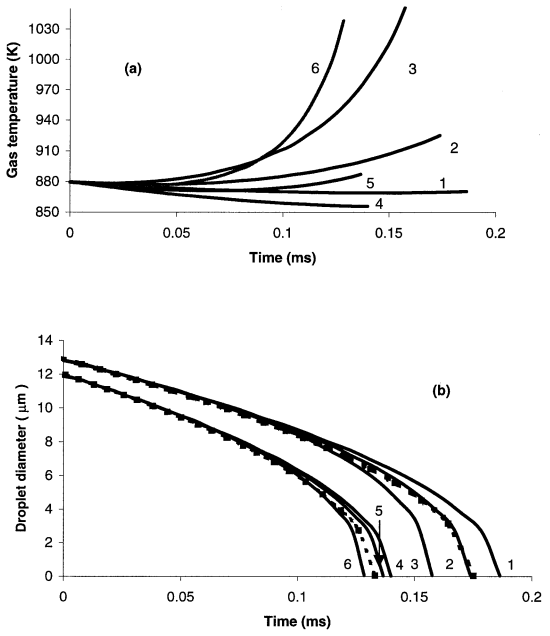

Fig. 4. (a) Plots of gas temperature versus time for T_s = 300 K [$A = 10^6$ 1/s (plot 1), $A = 5 \times 10^6$ 1/s (plot 2), $A = 10^7$ 1/s (plot 3)], and for T_s = 600 K [$A = 10^6$ 1/s (plot 4), $A = 5 \times 10^6$ 1/s (plot 5), $A = 10^7$ 1/s (plot 6)] as calculated from Eqs. (31) and (32). (b) Same as Fig. 4a but for droplet diameter versus time. Dotted curves calculated from Eqs. (35) and (36) (not distinguishable within the accuracy of plotting).

this figure, it is to be expected that Eq. 36 gives a reasonably good prediction of the dependence of droplet diameter on time. On the other hand, the values of A strongly influence the gas temperature, as can be seen from Fig. 4a. When $A = 10^6$ 1/s, the evaporation process clearly dominates over combustion. When $A = 5 \times 10^6$ 1/s and $A = 10^7$ 1/s the combustion becomes clearly visible at the end of evaporation. In all cases, however, in the initial stage evaporation dominates over combustion.

RESULTS OF THE CALCULATIONS BASED ON THE VECTIS CFD CODE

The results predicted by Fig. 4 are compared with those predicted by the CFD code VECTIS of Ricardo Consulting Engineers. In this code the governing equations for gas and droplets are solved in a self-consistent way, using the eulerian approach for the gas phase and the lagrangian approach for the droplets. All equations are solved in three dimensions. The VECTIS turbulence modelling is based on the conventional and RNG versions of the $k - \epsilon$ model. The Magnussen–Hjertager model and the more sophisticated two-zone flamelet models are available for high-temperature combustion. Because the present paper is focused on the autoignition processes, the simpler Magnussen–Hjertager model was used. Thermal radiation is modelled based on a slightly modified version of the conventional P-1 model [41]. In the customised version of the VECTIS code used in this paper the autoignition modelling is based on the Shell model [42].

The lagrangian approach models the spray as an ensemble of discrete droplets, which can break up, coalesce and interact stochastically

with turbulent structures. The time-dependent flowrate and initial droplet size distribution are specified. The droplet size distribution during spray development can be either taken to be an initial distribution specified by a user (no breakup) or calculated from one of the breakup models in the code. These are the Reitz–Diwakar model [43, 44], the Liu–Mather–Reitz model [45], and the Patterson–Reitz model [46]. Some of these models are discussed in [47]. The present analysis employed the Reitz–Diwakar model. The initial droplet size distribution does not need to be very accurate because the details of injection process are lost during the breakup and coalescence processes [43, 44]. Attention has been concentrated mainly on the analysis of the spray chemical autoignition process, rather than on the sensitivity of the results to the choice of the model for droplet breakup.

The parameters of the Shell model were taken as those for the primary reference fuel RON70 in the original formulation [42], except the coefficient A_{f4} describing the rate of production of the intemerdiate agent. The value of A was adjusted to give the best fit to available experimental data for n-heptane (see Appendix). The typical values recommended for this coefficient were between 3×10^6 and 6×10^6 [37] although sometimes a value 3×10^7 was preferred. In the analysis, three values of A_{f4} are used: 3×10^6, 6×10^6, and 3×10^7. The size of the domain (a cube) around a droplet has been chosen in such a way as to ensure that the mixture becomes stoichiometric once the droplet has evaporated. The walls of the domain have been taken to be adiabatic. In this case, the heat lost from the domain is exactly compensated by that gained from outside. Hence, the results are directly applicable to monodisperse sprays.

Plots of droplet diameter versus time for T_s = 600 K, T_s = 300 K and three values of A_{f4} are shown in Fig. 5a when radiation is taken into account, and when it is ignored. The dependence of droplet diameter on A_{f4} is rather weak, with no apparent effect for T_s = 600 K. This agrees with the result in Fig. 4b, that the coefficient A produces only a small influence on droplet diameter. Comparison of solid and dashed plots in Fig. 5a shows a clear influence of thermal radiation on droplet diameter. This also

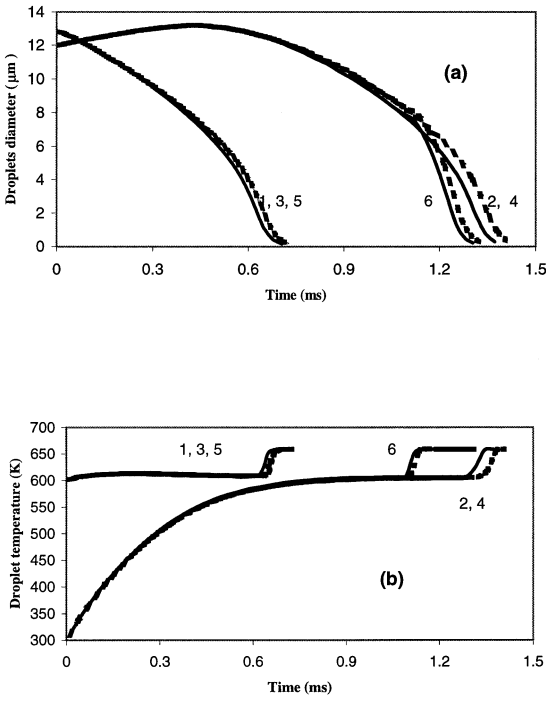

Fig. 5. (a) Droplet diameter versus time for initial gas temperature of 880 K, initial droplet temperature of 600 K, $A_{f4} = 3 \times 10^6$ (curve 1), $A_{f4} = 6 \times 10^6$ (curve 3), $A_{f4} = 3 \times 10^7$ (curve 5) and initial droplet temperature equal to 300 K, $A_{f4} = 3 \times 10^6$ (curve 2), $A_{f4} = 6 \times 10^6$ (curve 4), $A_{f4} = 3 \times 10^7$ (curve 6); solid curves for thermal radiation, dashed curves without radiation. (b) As (a) but droplet temperature versus time.

agrees with the prediction of the simplified Eqs. 36 and 37. Similar to Fig. 4b, Fig. 5a shows that the evaporation time for droplets with T_s = 600 K is about half that with T_s = 300 K. The evaporation time of droplets is about 5 to 8 times longer than given by the approximate formulae. Plots of droplet temperature versus time are shown in Figs. 5b for the same values of parameters as in Fig. 5a. The approximation of constant droplet temperature is reasonable for T_s = 600 K, but can be an oversimplification for T_s = 300 K. The periods of rapid increase in droplet temperature correspond to the times of explosion in the surrounding gas. These periods visibly depend on A_{f4}, but cannot be described by the qualitative model. The dependence of T_s on thermal radiation is small. Shortly before the droplet evaporates its temperature approaches the critical value. The treatment of the critical state in VECTIS assumes the specific heat of

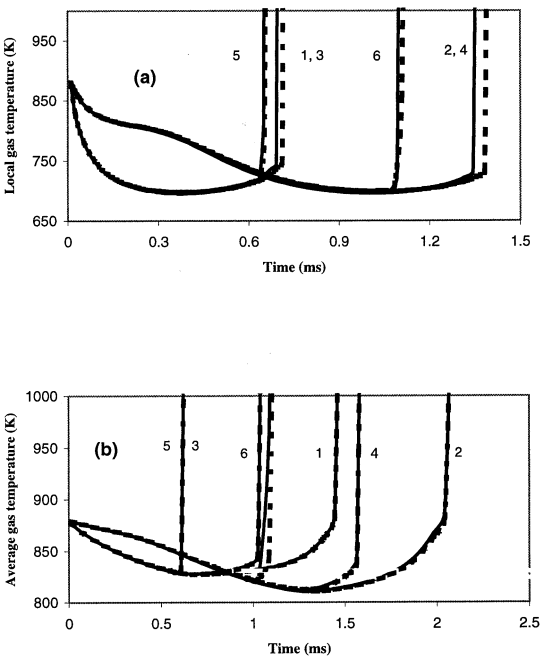

Fig. 6. (a) Plots of local gas temperature versus time: initial gas temperature of 880 K, initial droplet temperature of 600 K, $A_{f4} = 3 \times 10^6$ (curve 1), $A_{f4} = 6 \times 10^6$ (curve 3), $A_{f4} = 3 \times 10^7$ (curve 5) and initial droplet temperature of 300 K, $A_{f4} = 3 \times 10^6$ (curve 2), $A_{f4} = 6 \times 10^6$ (curve 4), $A_{f4} = 3 \times 10^7$ (curve 6); solid plots for thermal radiation, dashed curves without radiation. (b) As (a) but for the average gas temperature.

evaporation is equal to zero, without taking into account the modification of transport properties under these conditions [48–50]. This simplified approach is justified since the volume of droplets at this state is negligibly small compared with the initial volume (about 0.1% for plots 1, 3, 5 in Fig. 5b). Thus, any improvement in the treatment of droplet evaporation under critical conditions would have practically no effect on the overall accuracy of the model.

When considering the gas temperature, a distinction is made between the temperature in the immediate vicinity of droplets (in the computational cell in which the droplet is located) and the average temperature in the domain (averaged over all cells taking into account their sizes). The plots of these temperatures versus time for the same parameters as in Figs. 5a,b are shown in Figs. 6a,b. Because the interest is primarily in the initial stage of combustion these plots are restricted to temperatures under 1000 K. Initially both temperatures decrease, and the rate of this decrease is practically independent of A_{f4}. At a certain time, either before or after the complete evaporation of the droplet, both temperatures start to increase rapidly (gas explosion). The period of this increase appears to be a strong function of A_{f4}: increase in this parameter and allowance for radiation leads to a decrease in the time. Comparison of Figs. 6a and 6b shows that the local gas temperature is always below the global temperature before the explosion. The local temperature drops below 700 K, while the global temperature is always above 800 K. This reveals one of the main limitations of the qualitative model. This model was based on the assumption that the gas temperature in the vicinity of droplets is the same as the average temperature in the whole domain. On the other hand, the time of evaporation predicted by the model, including Eq. 37 is controlled by the difference between the average gas temperature, rather than the local one. It is believed that this is the main reason for the descrepancy between the droplet evaporation time predicted by the qualitative model and the CFD code. This is shown by the plot of evaporation time $t_{\mathrm{evap}(0)}$ versus gas initial temperature for $T_s = 600$ K in Fig. 7a. When $T_{g0} \approx 900$ K, $t_{\mathrm{evap}(0)} \approx 0.13$ ms, in agreement with Fig. 4b. On the other hand, when T_{g0} falls to about 670 K then $t_{\mathrm{evap}(0)} \approx 0.7$ ms, in agreement with the CFD prediction (see Fig. 5a). This result is certainly data-specific. A similar analysis for other fuels is beyond the scope of this paper, although we anticipate that similar conclusions could be obtained for them.

Figure 7b presents a plot of κ versus temperature. This coefficient is a relatively weak function of gas temperature, with a value close to 0.01. This is consistent with the results shown in Fig. 5a and indicates that the radiative corrections for these values of parameters are close to 1%. These radiative corrections can be considerably larger for larger droplets, higher gas temperatures and small values of gas thermal conductivity. Hence, they must be taken into account in practical analyses.

In Figs. 8a,b plots, similar to those shown in Figs. 4a,b but for $T_{g0} = 670$ K and the droplet temperatures 600 K, are presented. The droplet evaporation time is close to 0.8 ms, in agreement with Fig. 5a. This time is a rather weak

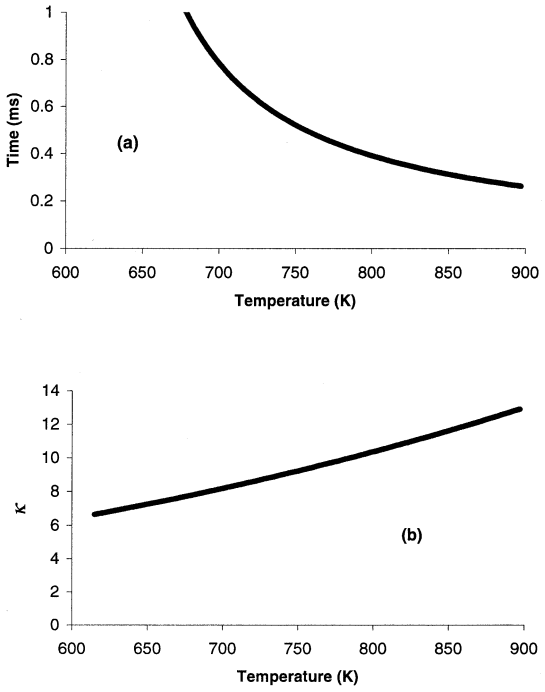

Fig. 7. (a) Plot of $t_{evap(0)}$ versus gas temperature. (b) Plot of κ in Eq. (37) versus gas temperature.

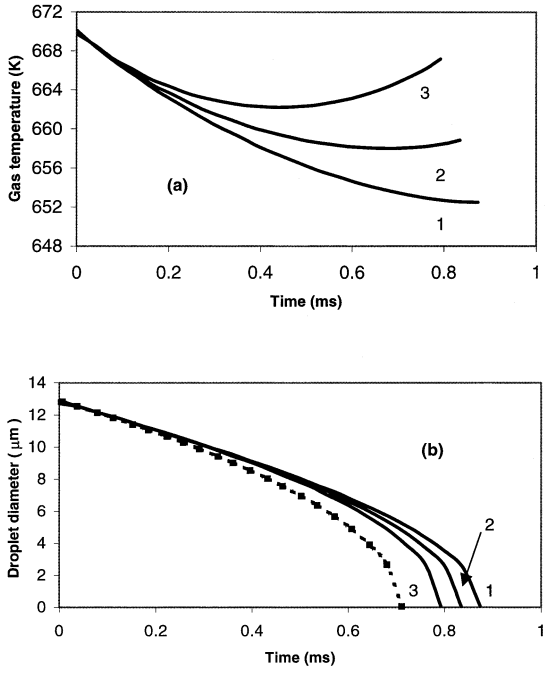

Fig. 8. (a) Plots of the local gas temperature versus time: initial gas temperature of 670 K, initial droplet temperature of 600 K, $A_{f4} = 3 \times 10^6$ (curve 1), $A_{f4} = 6 \times 10^6$ (curve 2), $A_{f4} = 3 \times 10^7$ (curve 3) (with thermal radiation). (b) As (a) but for the droplet diameter.

function of A, similar to the case shown in Fig. 4b. On the other hand, the value of A strongly influences the values of gas temperature, as shown in Fig. 8a. The initial decrease of this temperature indicates that the heat for evaporation dominates over the heat produced during combustion. This agrees with the predictions shown in Figs. 6a.

CONCLUSIONS

Results of a qualitative analysis of evaporation and ignition of liquid fuel droplets in monodisperse sprays in the presence of convective and radiative heat exchanges with the surrounding hot gas, have been presented. The radiative energy exchange between fuel droplets surface and gas is described using the P-1 model with Marshak boundary conditions. The system of equations describing the effects of heating, evaporation and combustion of fuel droplets is simplified assuming that the Nusselt and Sherwood numbers to be equal to 2. The chemical term is presented in the Arrhenius form with a pre-exponential factor calculated from the enthalpy equation using the Shell autoignition model, with the parameters corresponding to the primary reference fuel RON70. Three values of the pre-exponential factor are employed for the rate of production of the intermediate agent: 3×10^6, 6×10^6, and 3×10^7. The resultant singularly perturbed system of ordinary differential equations is analysed based on the geometrical version of the integral manifold method. The ignition process is subdivided into two stages: droplet evaporation and ignition of gaseous mixture. The basic system of equations is eventually reduced to the system of just two equations: one for the normalized gas temperature and another for the normalized droplet radii. These equations are further simplified assuming that the changes of gas temperature are small, which is justified in the initial stages of the combustion process. Results predicted by the analytical solutions are compared with the results predicted by the CFD package VECTIS. The analytical solution underpredicts the evaporation time. A considerably better agreement between the evaporation times predicted by

CFD and the qualitative theory is achieved when the gas temperature is assumed to be equal to the local temperature in the vicinity of droplets. The effects of thermal radiation are noticeable, especially at high temperatures, and large droplets and cannot be ignored.

The authors are grateful to Dr. E. Sazhina for her help in running the VECTIS CFD calculations and the preparation of Figs. 5, 6, and 9, and to L. Alger for his contribution in the preparation of Fig. 9. Ricardo Consulting Engineers is acknowledged for its financial and technical support. S. Sazhin is grateful to the Academic Study Group in London (UK) and the Ben–Gurion University of the Negev (Israel) for financial support on his visit to Israel in March 1999, when the reported work began. I. Goldfarb is grateful to the Royal Society for financial support on his visit to the University of Brighton in October 2000 when the work on this paper was completed.

REFERENCES

1. Kuo, K. K., *Principles of Combustion*, John Wiley & Sons, New York, 1986.
2. Stone, R., *Introduction to Internal Combustion Engines*, MacMillan, New York, 1992.
3. Aggarwal, S. K., *Prog. Energy Combust. Sci*. 24:565 (1998).
4. Chiu, H. H., and Hu, L. H., *27th International Symposium on Combustion*, The Combustion Institute, Pittsburgh, 1999, p. 1889.
5. Stapf, P., Dwyer, H. A., and Maly, R. R., *Twenty-Seventh International Symposium on Combustion*, The Combustion Institute, Pittsburgh, 1999, p. 1857.
6. Babushok, V. I., and Gol'dshtein, V. M., *Combust. Flame* 72:221 (1988).
7. Gol'dshtein, V., and Sobolev, V., In *Singularity theory and some problems of functional analysis*, American Mathematical Society, Series 2, 153:73 (1992).
8. Goldfarb, I., Gol'dshtein, V., Kuzmenko, G., and Greenberg, J. B., *Proceedings of ASME Heat Transfer Division* 2:199 (1997).
9. Goldfarb, I., Gol'dshtein, V., Kuzmenko, G., and Greenberg, J. B., *Twenty-Seventh International Symposium on Combustion*, The Combustion Institute, Pittsburgh, 1998, p. 2367.
10. McIntosh, A. C., Gol'dshtein, V., Goldfarb, I., and Zinoviev, A., *Combust. Theory and Modelling* 2:153 (1998).
11. Incroperra, F. P., and DeWitt, D. P., *Fundamentals of Heat and Mass Transfer*, John Wiley & Sons, New York, 1996.
12. Chang, S. L., and Rhee, K. T., *SAE paper 831332*, 1983.
13. Chapman, M., Friedman, M. C., and Aghan, A., *SAE paper 831725*, 1983.
14. Mengüc, M. P., Viskanta, R., and Ferguson, C. R., *SAE paper 850503*, 1985.
15. Viskanta, R., and Mengüc, M. P., *Prog. Energy Combust. Sci*. 13:97 (1987).
16. Lage, P. L. C., and Rangel, R. H., *J. Thermophysics and Heat Transfer* 7:502 (1993).
17. Siegel, R., and Howell, J. R., *Thermal Radiation Heat Transfer*, Hemisphere Publishing Corporation, Washington, 1992.
18. Modest, M. F., *Radiative Heat Transfer*, McGraw–Hill, 1993.
19. Sazhin, S. S., Sazhina, E. M., Faltsi–Saravelou, O., and Wild, P., *Fuel* 75:289 (1996).
20. Goldfarb, I., Gol'dshtein, V., Kuzmenko, G., and Sazhin, S. S., *Combust. Theory Modelling* 3:769 (1999).
21. Marshak, R. E., *Phys. Rev*. 71:443 (1947).
22. Chang, K.-C., and Shieh, J.-S., *Int. J. Heat Mass Transfer* 38:2611 (1995).
23. Dombrovsky, L. A., *Int. J. Heat Mass Transfer* 43:1661 (2000).
24. Dombrovsky, L. A., *Radiation Heat Transfer in Disperse Systems*, Begell House Inc, New York, Wallingford (UK), 1996.
25. Westbrook, C. K., and Dryer, F. L., *Combust. Sci. Technol*. 27:31 (1981).
26. Bergeron, C. A., and Hallett, W. L. H., *The Canadian J. Chem. Eng*. 67:142 (1989).
27. Spalding, D. B., *Some Fundamentals of Combustion*, Academic Press, New York, 1955.
28. Williams, A., *Combustion of Liquid Fuel Sprays*, London, Butterworths, 1990.
29. Bird, R. B., Stewart, W. E., and Lightfoot, E. N., *Transport Phenomena*, John Wiley & Sons, New York, 1960.
30. Mills, A. F., *Heat and Mass Transfer*, Richard D. Irwin, Inc, 1995.
31. Semenov, N. N., *Z. Phys*. 48:571–581 (1928).
32. Frank–Kamenetskii, D. A., *Diffusion and Heat Exchange in Chemical Kinetics*, 2nd ed., Plenum Press, New York, 1969.
33. Mitropolskii, Ju. A., and Likova, O. B., *Integral Manifolds in Nonlinear Mechanics*, Novosibirsk, Nauka, 1973 (in Russian).
34. Strygin, B. B., and Sobolev, V. A., *Decomposition of Motions by the Integral Manifolds Method*, Moscow Nauka, 1988 (in Russian).
35. Fenichel, N., *J. Differential Equations* 31:53 (1979).
36. Babushok, V. I., Gol'dshtein, V. M., and Sobolev, V. A., *Combust. Sci. Technol*. 70:81 (1990).
37. Sazhina, E. M., Sazhin, S. S., Heikal, M. R., and Marooney, C., *Fuel* 78:389 (1999).
38. Sazhina, E. M., Sazhin, S. S., Heikal, M. R., Babushok, V. I., and Johns, R., *Combust. Sci. Technol*. 160:317 (2000).
39. Dec, J. E., *SAE paper 970873*, 1997.
40. Flynn, P. F., Durrett, R. P., Hunter, G. L., zur Loye, A. O., Akinyemi, O. C., Dec, J. E., and Westbrook, C. K., *SAE paper 1999-01-0509*, 1999.

41. Sazhin, S. S., Sazhina, E. M., and Heikal, M. R., *Fuel* 79:1843–1852 (2000).
42. Halstead, M. P., Kirsch, L. J., and Quinn, C. P., *Combust. Flame* 20:211 (1977).
43. Reitz, R. D., and Diwakar, R., *SAE Paper 860469*, 1986.
44. Reitz, R. D., and Diwakar, R., *SAE Paper 870598*, 1987.
45. Liu, A. B., Mather, D., and Reitz, R. D., *SAE Paper 930072*, 1993.
46. Patterson, M. A., and Reitz, R. D., *SAE Paper 980131*, 1998.
47. Borman, G. L., and Ragland, K. W., *Combustion Engineering*, WCB and McGraw–Hill, New York, 1998.
48. Vesovic, V., and Wakeham, W. A., In *Supercritical Fluid Technology: Reviews in Modern Theory and Applications* (T. J. Bruno and J. F. Ely, Eds.), CRC Press, Boca Raton, FL, 1991, pp. 245–289.
49. Binney, J. J., Dowrick, N. J., Fisher, A. J., and Newman, M. E. J., *The Theory of Critical Phenomena: An Introduction to the Renormalization Group*, Clarendon Press, Oxford, 1992.
50. Arias–Zugasti, M., Garcia-Ybarra, P. L., and Castillo, J. L., *Phys. Rev. E* 60:2930 (1999).
51. Pitsch, H., and Peters, N., Investigation of the ignition process of sprays under Diesel engine conditions using reduced n-heptane chemistry, *SAE2464* (1998).

Received 14 October 1999; revised 1 November 2000; accepted 5 November 2000

APPENDIX: CALCULATION OF THE PRE-EXPONENTIAL FACTOR A

One of the most serious limitations of the model is the assumption about the Arrhenius form of the chemical terms in Eqs. (1) and (3). In reality, the form of these terms is far more complicated and involves hundreds of competing chemical reactions. In the case of diesel fuel droplets ignition, these reactions can be reasonably approximated by the Shell model [37]. At the same time, the presentation of the chemical term in the form more complicated than the Arrhenius one makes the whole problem untractable by analytical methods.

A compromise is sought between the accuracy and simplicity of the presentation of the chemical term. The approach is based on a rigorous calculation of T_g by using the commercial CFD code VECTIS with the Shell model implemented in it. Droplets of n-dodecane and gas are considered with the initial parameters given earlier. The gas temperature close to the droplets is different from that remote from them. The average temperature in the domain is T_g. The concentration of droplets is chosen to provide a near stoichiometric mixture (air/fuel mass ratio equal to 11.7) once the droplets have evaporated.

Once values of T_g as functions of time have been calculated, they are substituted into Eq. (1) and the values of A can be found as:

$$A = \frac{\rho_g C_{pg} \alpha_g \dfrac{dT_g}{dt} + 4\pi R_d^2 n h (T_g - T_s) + 4\pi R_d^2 n \sigma \epsilon_1 (T_g^4 - T_s^4)}{\eta c'_{ff} \mu_f \alpha_g Q_f \exp\left(-\dfrac{E}{R_u T_g}\right)}. \quad \text{(A1)}$$

In Eq. (A1) all the parameters except E and A are either known parameters of the system or calculated values (T_g). Thus Eq. (A1) allows pairs of values of A and E to be specified which satisfy Eq. (1) at any instant. To simplify the problem, following [26], $E = 76$ kJ/mol.

Because experimental data for the chemical autoignition delay for n-dodecane are not available, those for n-heptane are used, following [37]. This assumption is similar to that in [51] although there are the differences in fuel properties. Ignition time delays for premixed n-heptane predicted by [37] using the kinetic rate parameters corresponding to the Primary Reference Fuel RON70 show good agreement with experimental results when A_{f4} (pre-exponential factor in the rate of production of the intermediate agent) is in the range between 3×10^6 and 6×10^6 [37].

The results of calculations of A are shown in Fig. 9 for $A_{f4} = 3 \times 10^6$, $A_{f4} = 6 \times 10^6$, and $A_{f4} = 3 \times 10^7$ and initial droplet temperatures equal to 300 K and 600 K. Although the third value of A_{f4} is beyond the range of A_{f4} recom-

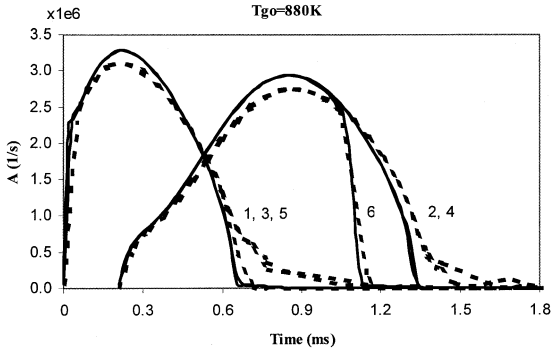

Fig. 9. Plots of pre-exponential factor A versus time as calculated from Eq. (A1) for initial gas temperature of 880 K, initial droplet temperature of 600 K, $A_{f4} = 3 \times 10^6$ (curve 1), $A_{f4} = 6 \times 10^6$ (curve 3), $A_{f4} = 3 \times 10^7$ (curve 5) and initial droplet temperature of 300 K, $A_{f4} = 3 \times 10^6$ (curve 2), $A_{f4} = 6 \times 10^6$ (curve 4), $A_{f4} = 3 \times 10^7$ (curve 6); solid curves for thermal radiation, dashed curves without thermal radiation.

mended in [37] it is included to investigate the sensitivity of the results to the choice of A_{f4}. As can be seen from this figure, A is a rather strong function of time and the approximation of a constant value of A is generally not valid. The rapid decrease of A during and after explosion reflects the rapid increase of T_g in the exponential term in the denominator in the right of Eq. (A1). Because account cannot be taken of the temporal variations of A this dependence is allowed for by using 3 values of A: $A = 10^6$ 1/s; $A = 5 \times 10^6$ 1/s and $A = 10^7$ 1/s.